SUPPLEMENTARY DATA

The proposed design of the unidimensional photonic crystal (1D PC) in absence of the defect layer used in the current study is represented schematically in Figure S1.

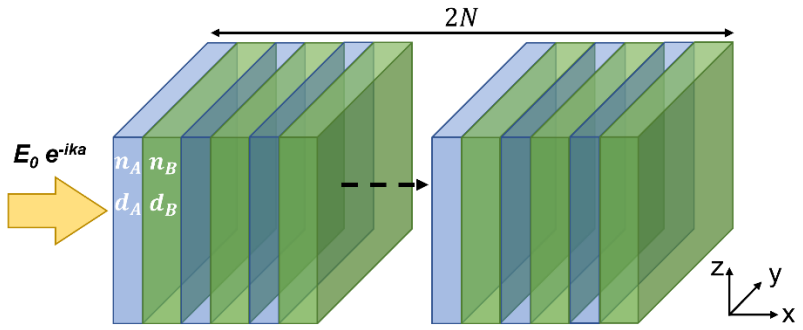

Figure S1. Schematic of the proposed 1D photonic crystal.

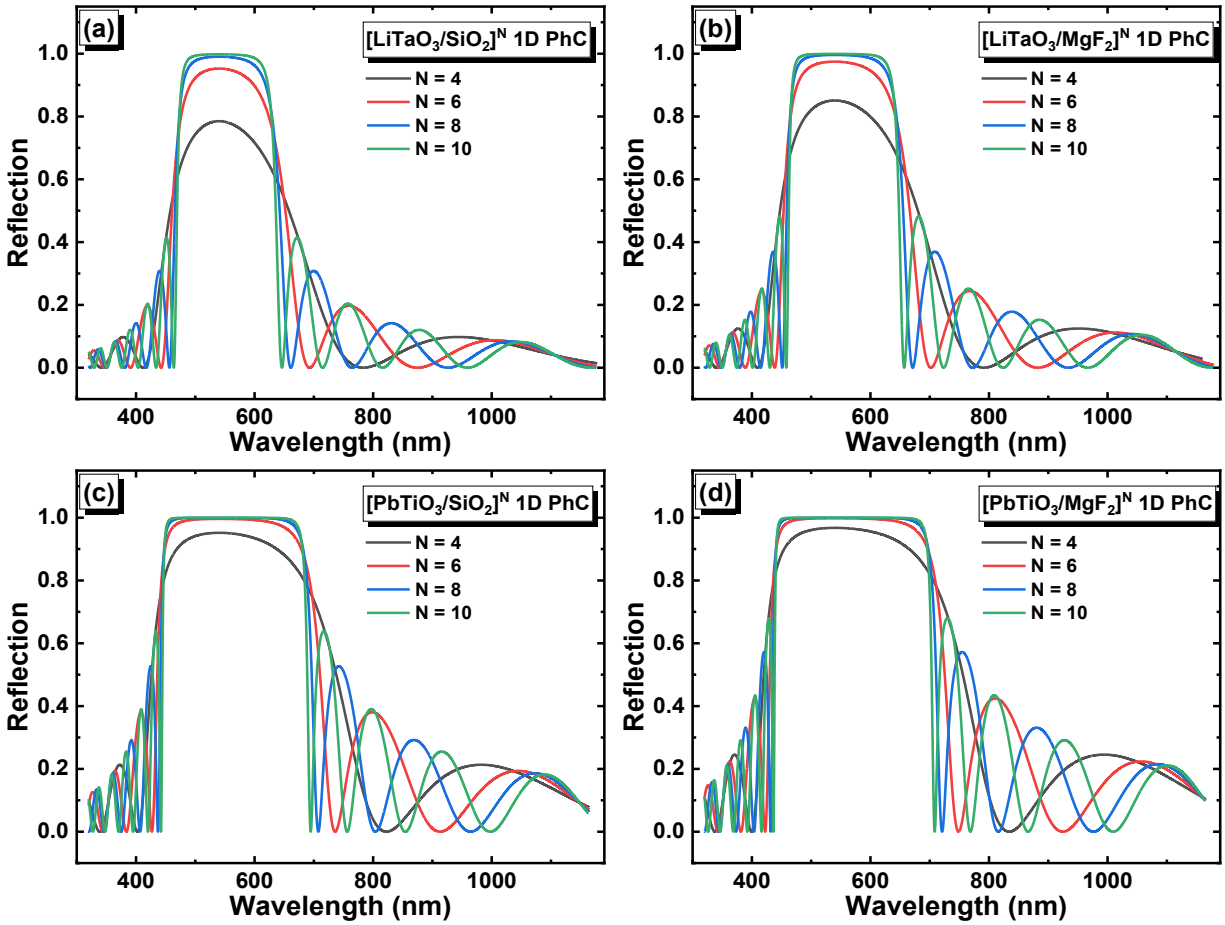

Figure S2. Wavelength and period number dependence of the reflection in different structures.

The reflection and the transmittance was calculated as a function of the wavelength and number of period in $[LiTaO_3/SiO_2]^N$, $[LiTaO_3/ MgF_2]^N$, $[PbTiO_3/ SiO_2]^N$ and $[PbTiO_3/ MgF_2]^N$ structures are shown in Figure S2 and S3. As seen, a number of 10 repetition period is needed to obtain well-defined photonic bandgap in $[LiTaO_3/SiO_2]^N$ and $[LiTaO_3/ MgF_2]^N$, and a minimum number of 8 is needed to obtain well-defined photonic bandgap in $[PbTiO_3/ SiO_2]^N$ and $[PbTiO_3/ MgF_2]^N$.

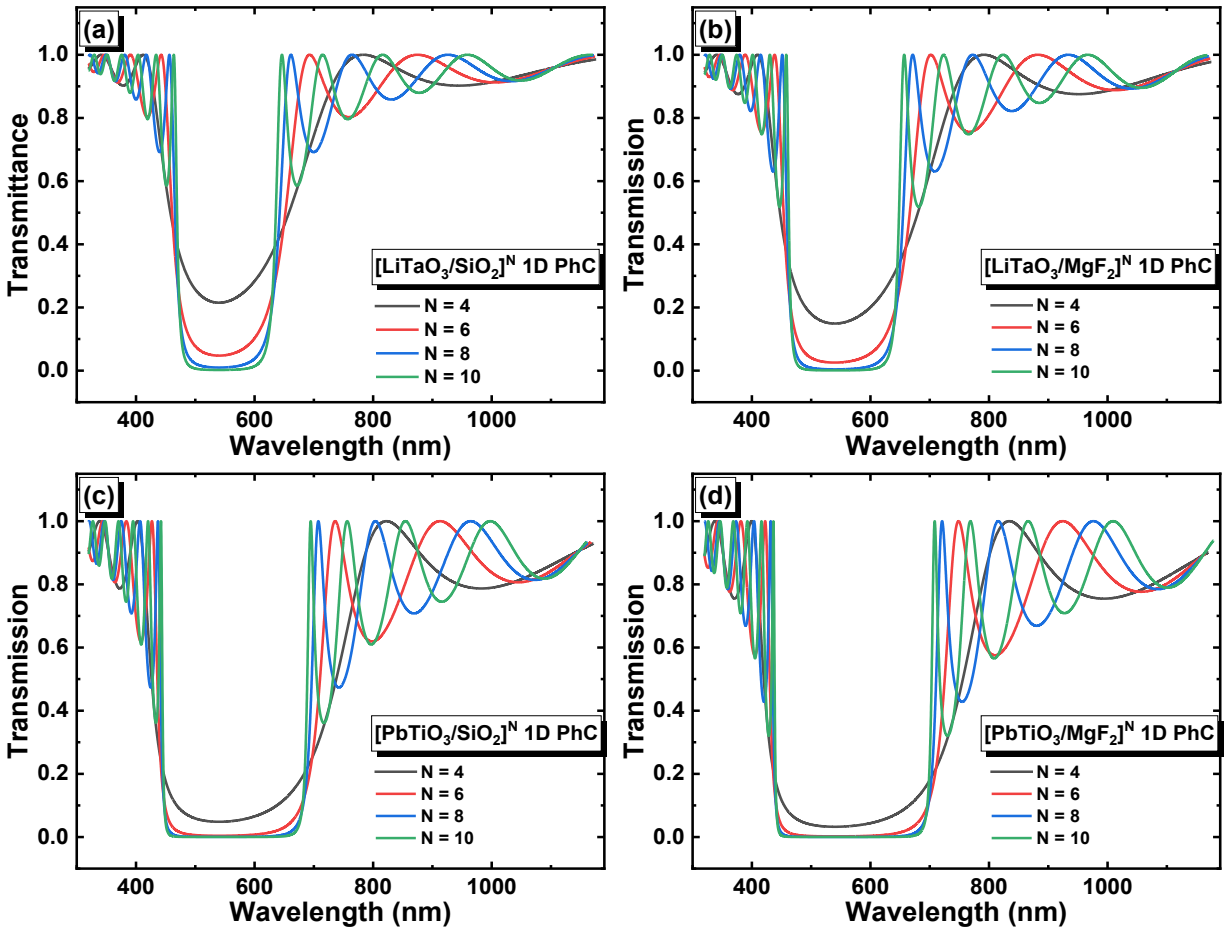

Figure S3. Wavelength and period number dependence of the transmittance in different structures.

The dependence of photonic band gaps in $[LiTaO_3/SiO_2]^{10}$, $[LiTaO_3/ MgF_2]^{10}$, $[PbTiO_3/ SiO_2]^{10}$ and $[PbTiO_3/ MgF_2]^{10}$ structures on the incidence angle of light can be observed from the transmittance maps in the case of TE polarization mode (Figure S4) and TM polarization mode (Figure S5). As seen in Figure S4, the photonic band gaps widen as the incidence angle increases from zero to 89 degrees. However, they narrow as the incidence angle increases to 89 degrees in the case of TM polarization mode (Figure S5).

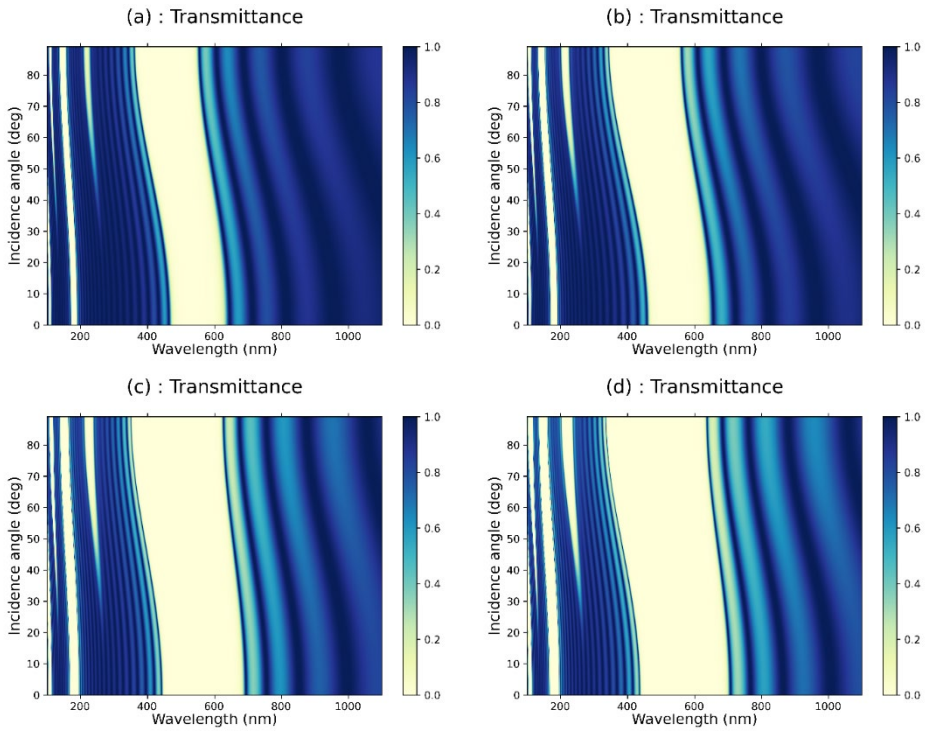

Figure S4. Transmittance map in **(a)** $[LiTaO_3/SiO_2]^{10}$, **(b)** $[LiTaO_3/ MgF_2]^{10}$, **(c)** $[PbTiO_3/ SiO_2]^{10}$ and **(d)** $[PbTiO_3/ MgF_2]^{10}$, in the case of TE polarization mode.

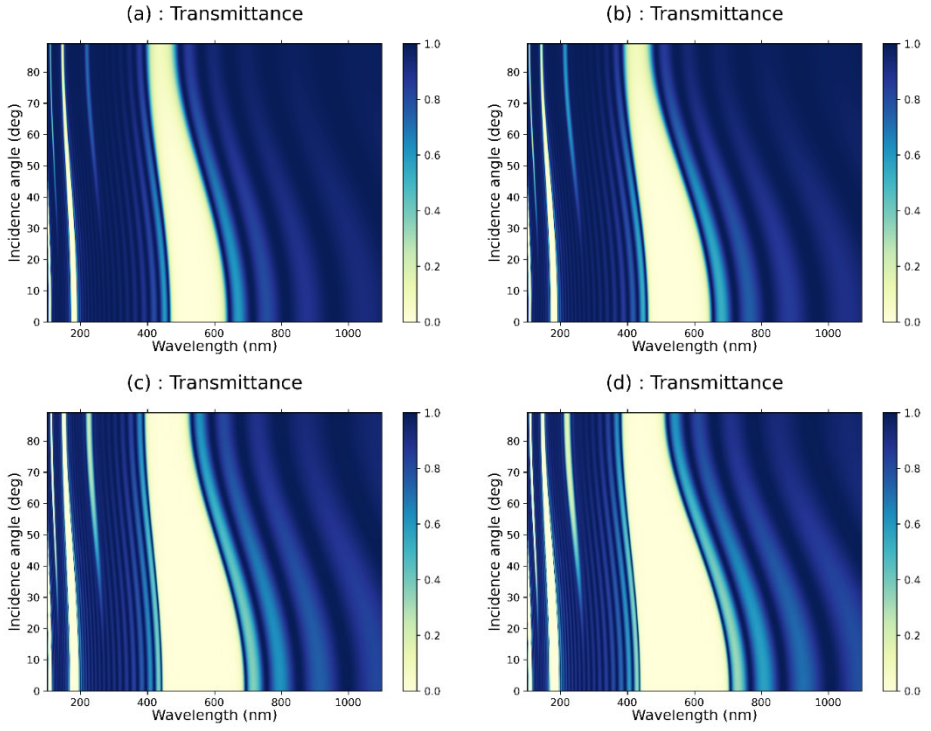

Figure S5. Transmittance map in **(a)** $[LiTaO_3/SiO_2]^{10}$, **(b)** $[LiTaO_3/ MgF_2]^{10}$, **(c)** $[PbTiO_3/ SiO_2]^{10}$ and **(d)** $[PbTiO_3/ MgF_2]^{10}$, in the case of TM polarization mode.

Figures S6a to d show the transmittance maps as a function of the wavelength and incidence angle of light through the structures $[TiLaO_3/SiO_2]^5D[TiLaO_3/SiO_2]^5$, $[TiLaO_3/MgF_2]^5D[TiLaO_3/MgF_2]^5$, $[PbTiO_3/SiO_2]^5D[PbTiO_3/SiO_2]^5$, and $[PbTiO_3/MgF_2]^5D[PbTiO_3/MgF_2]^5$ referred as structure 1, structure 2, structure 3 and structure 4. The transmittance was measured with the assumption that the nanochannel has a thickness of 600 nm and it is filled with distilled water (n_{water} = 1.333). Double resonant mode was observed in structure 1 and structure 2. As seen in Figure S6c and Figure S6d, structure 3 and 4 showed three resonant peaks.

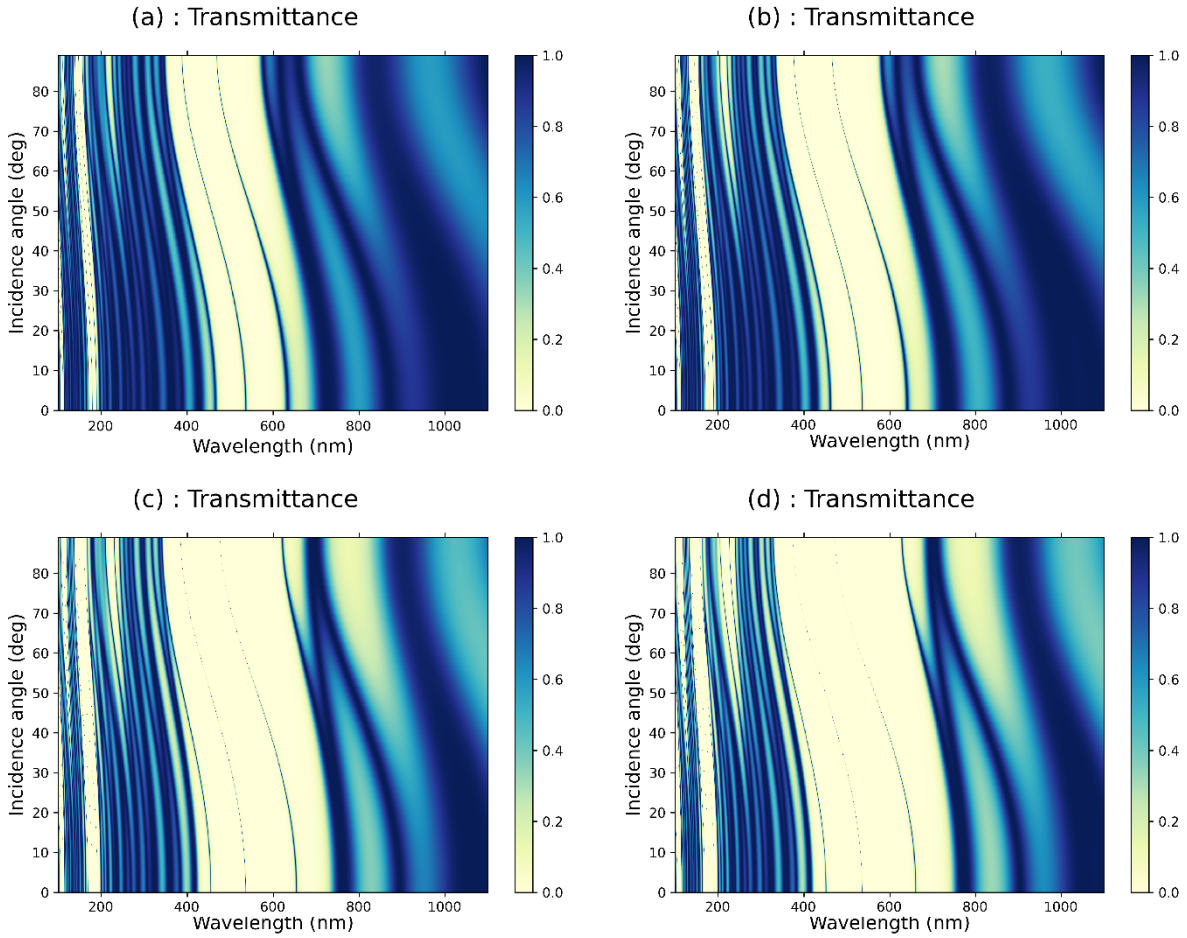

Figure S6. Variation of the transmittance as a function of the wavelength and incidence angle of light in **(a)** structure 1, **(b)** structure 2 **(c)** structure 3 and **(d)** structure 4 (defect layer d = 600 nm, and n_{water} = 1.333)

We investigated the shift of the resonant peaks at d = 420 nm and incidence angle of 60 degrees with respect to Fresh urinary EV (U-EV), Activated platelets EV (AP-EV), Neuroblastoma EV (N-EV), and Blood EV (B-EV), please refer to Figure S7. Similar to the behavior observed in Figure 4 in the manuscript, peaks shift to longer wavelengths as the refractive index increases. In addition, peaks are wide in the 1D PC-BIO structure 1 and narrow in the case of 1D PC-BIO

structure 4, translating the better biosensing performance of $[PbTiO_3/MgF_2]^5D[PbTiO_3/MgF_2]^5$ 1D PC-BIO compared with other structures.

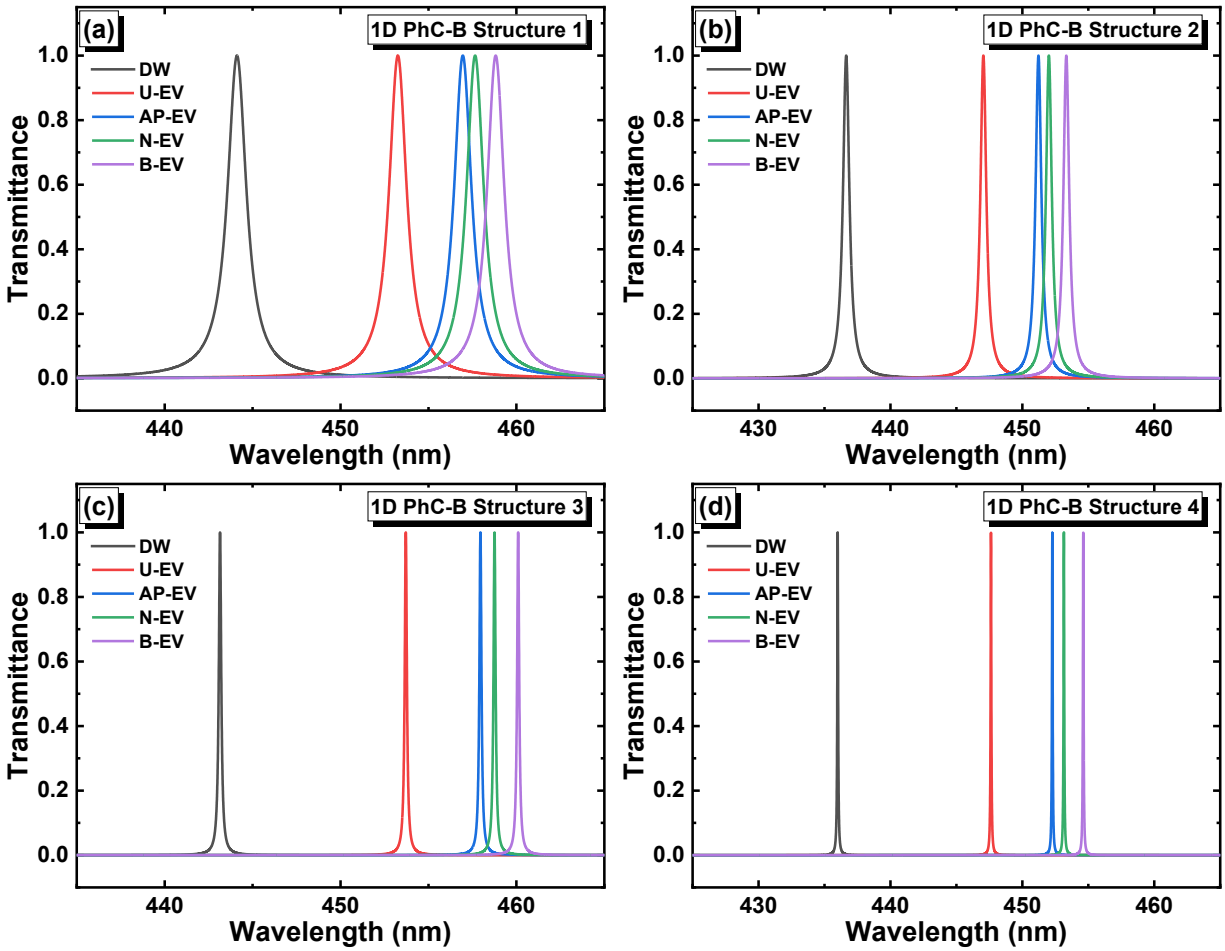

Figure S7. Shift in defect mode position with respect to various EVs samples at incidence angle of light of 60 degrees in **(a)** structure 1, **(b)** structure 2, **(c)** structure 3 and **(d)** structure 4.

From the defect mode shifts (Figure S7), we deduced the biosensors' performances as shown in Table S1. The values of the sensitivity, the figure of merit and the Q factor, are represented graphically in Figure S8

Table S1. The biosensing performance of 1D PC-BIOs at d = 420 nm and incidence angle of 60°.

		U- EV	AP-EV	N-EV	B-EV
$S(nm/RIU)$	Structure 1	222.95	225.26	225.65	226.29
	Structure 2	253.61	255.74	256.10	256.71
	Structure 3	257.71	259.79	260.15	260.82
	Structure 4	283.46	285.42	285.80	286.38
$FOM\ (RIU^{-1})$	Structure 1	185.23	190.09	190.85	192.02
	Structure 2	474.44	485.61	487.24	489.68
	Structure 3	1773.87	1843.13	1854.24	1873.40
	Structure 4	4487.31	4655.38	4689.09	4725.82
Q factor	Structure 1	376.56	385.60	387.06	389.33
	Structure 2	836.31	856.81	859.97	864.71
	Structure 3	3123.02	3249.05	3269.81	3304.83
	Structure 4	7085.99	7376.76	7434.75	7501.90

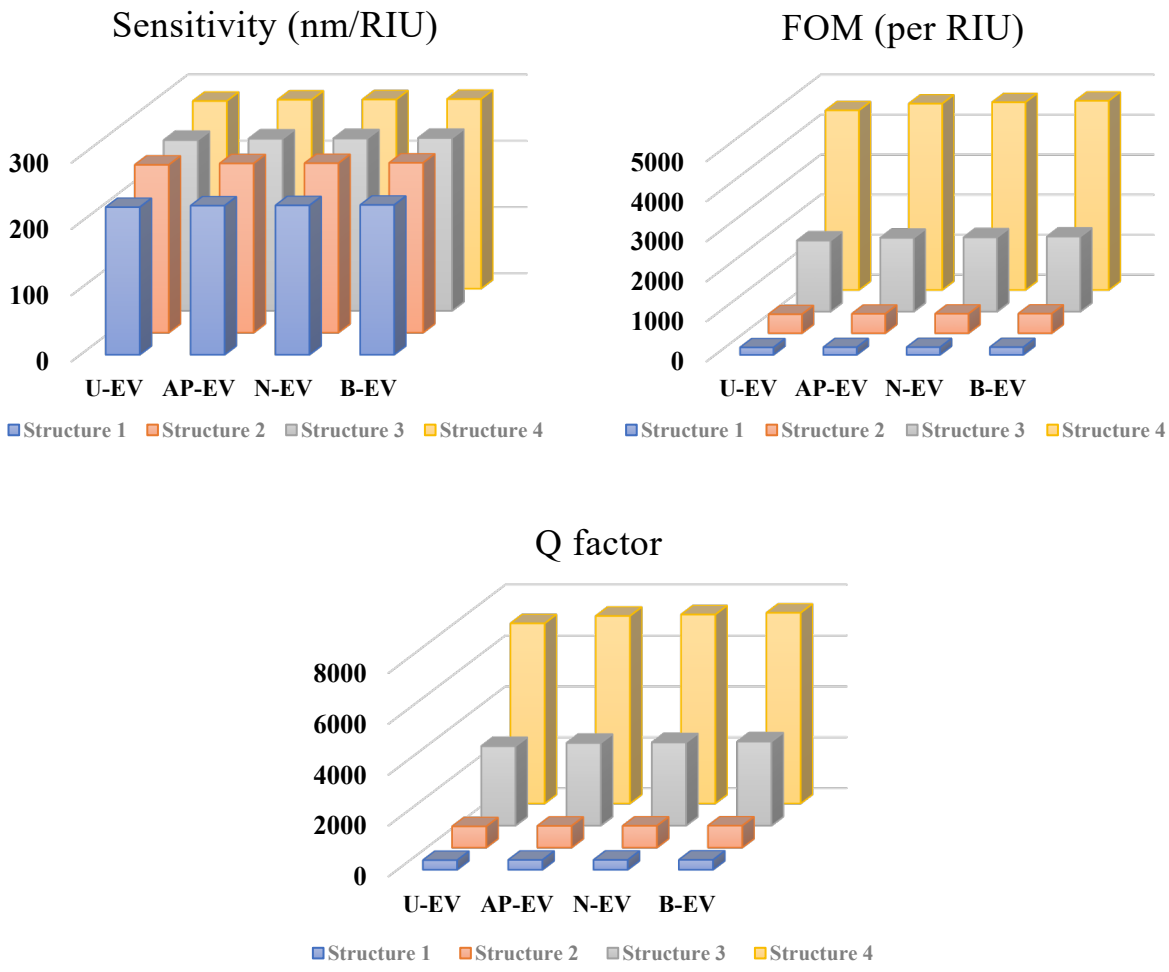

Figure S8. The performance of the 1PC-BIOs at incidence angle of light of 60 degrees.